ELSEVIER

Polymer 43 (2002) 6429–6438

polymer

www.elsevier.com/locate/polymer

Comparison of the effect of reactive and non-reactive steric stabilisers on the mechanism of film formation in methyl methacrylate/butyl acrylate copolymers latexes. Part 2. Electrical conduction and dielectric spectroscopic investigations

Lynda A. Cannon, Richard A. Pethrick*

Department of Pure and Applied Chemistry, University of Strathclyde, Thomas Graham Building, 295 Cathedral Street, Glasgow G1 1XI, UK

Received 16 April 2002; received in revised form 30 July 2002; accepted 7 August 2002

Abstract

A comparison of the film forming ability of methyl methacrylate (MMA)/butyl acrylate (BA) latex copolymers stabilised by either a reactive or a non-reactive steric stabiliser is reported and indicates the key role of the degree of polymerisation of the hydrophilic ethylene oxide chain on the coalescence process. The study uses dielectric measurements to follow and identify the various stages of film formation. The ability of the stabiliser to segregate and diffuse from the interfacial layer into the surrounding media influences in both the rate of the coalescence process and the final physical properties of the films formed. Dielectric relaxation and electrical conductivity measurements indicate the mechanistic complexity of the coalescence process and illustrate that the clear differences exist between the behaviour of the two systems investigated. A model for the film formation processes is presented which incorporates the various features identified by the dielectric study. © 2002 Published by Elsevier Science Ltd.

Keywords: Latex; Film formation; Dielectric spectroscopy and electrical conductivity

1. Introduction

In Part 1, investigations of the coalescence of methyl methacrylate (MMA)/butyl acrylate (BA) latex copolymers stabilised by either a reactive or a non-reactive steric stabiliser were reported [1]. The rate and degree of coalescence was observed to depend on the effects of constraints on the stabiliser and role of the length of the hydrophilic ethylene oxide chain. The ability of the stabiliser to segregate and diffuse from the interfacial layer into the surrounding media influences both the rate of the coalescence process and the final physical properties of the films formed. Differential scanning calorimetry and dynamic mechanical analysis indicated the mechanism of the coalescence process is complex and clearly identifies differences between the behaviour of these two systems. The final structure of the films was investigated using atomic force microscopy and revealed the extent to which coalescence of the latex particles had occurred. Previously [2], the application of dielectric measurements to the characterisation of the film formation process has allowed identification of distinct stages in the coalescence process. The mechanism for coalescence was found to depend upon the glass transition temperature (T_g) of the studies of 2-ethylhexylacrylate/methyl methacrylate copolymer latexes have shown that the mechanism for coalescence depended upon the T_g of the latex [2–16]. A comparison of the effect of variation of chain length for latexes stabilised using nonylphenol ethoxylate (NPX), (where X designates the average chain length of the ethoxylate chain) indicated that NP20 was able to facilitate coalescence whereas NP30 and NP40 inhibited coalescence [2]. The longer chains were able to form a crystalline structure in the interfacial region. In general, evaporation of water is the dominant rate limiting process in the initial stages of film formation, when the temperature of the latex is 20 K or more above its T_g. When the latex is near to T_g of the copolymer, the rate controlling step for film formation involves deformation of the spherical emulsion particles. Evaporation rates are

* Corresponding author. Tel.: +44-141-548-2260; fax: +44-141-548-4822.

E-mail address: r.a.pethrick@strath.ac.uk (R.A. Pethrick).

0032-3861/02/$ - see front matter © 2002 Published by Elsevier Science Ltd.
PII: S0032-3861(02)00541-4

Table 1
Characteristics of latex materials

Latex-code	% Non-volatiles	MFFT (K)	Mean particle diameter (nm)	T_g (K) DSC	M_w	M_n
1035-RS	45	291	156	285	61,100	91,750
1035-NP20	52	291	191	287	161,500	150,500

retarded in a latex system that can undergo extensive particle deformation [13] and correlation has been observed between the film formation characteristics and T_g of the polymer.

Reactive and non-reactive steric stabilisers may be differentiated according to their ability to be chemically incorporated during synthesis into the latex material. The mixed hydrophilic–hydrophobic nature of the surfactant, causes the molecules to segregate to the particle surface and the disordered poly(ethyleneoxide) (PEG) segment provide a steric barrier to coalescence of the particles when dispersed in aqueous media. As a result of chemical reaction, the reactive surfactant can be polymerised into the matrix and locked into the surface layer of the particle. This study compares the film forming behaviour of a reactive and non-reactive steric stabiliser. The two surfactants selected for investigation are:

Synperonic NP20 (steric)

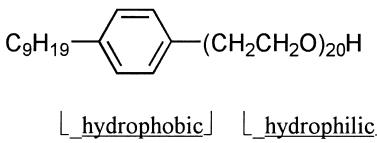

and

Reactive surfactant (steric) $n = 16–20$

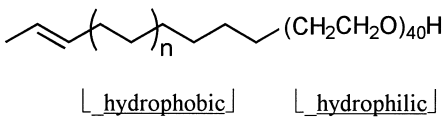

Although the hydrophobic segments are different in the above molecules their solubility in the monomers will be very similar and will not influence significantly the initial distribution of the segments between the organic and aqueous phases. The surfactants have comparable structures, but they have different lengths of hydrophilic. Recently it has been shown that PEG chains impart an attractive force to approaching particles [17]. This study aims to explore the use of dielectric measurements for the characterisation of coalescence in a system stabilised either by a reactive or non-reactive stabiliser and determine whether the immobilisation of the surfactant and its chemical structure has an effect on the film formation process.

2. Experimental

2.1. Materials—latex preparation and chemical characterisation

Two methyl methacrylate (MMA)/butyl acrylate (BA) latex copolymers have been detailed in Part 1 [1]. The codes used are 1035-RS for the reactive surfactant and 1035-NP20 for the synperonic stabilised emulsion system. The chemical characteristics of the latexes used in this paper are described in Part 1 and are summarised in Table 1. The concentration of surfactant used approximates to 85% of monolayer coverage at the measured particle size, Table 1. The extent to which the reactant surfactant was incorporated in the beads was investigated by extraction of the experiments on the beads. NMR analysis of the eluent obtained from dialysis could detect no free reactive surfactant.

2.2. Physical characterisation of the latex film

The latex films were characterised using the following techniques.

2.2.1. Stage one of film formation

The transformation of emulsion into a solid film was followed by conductance measurements.

Conductance measurements. Dissolved ions give the latex dispersion a high initial conductivity. As the latex dries, the loss of water causes the ion concentration and hence the electrical conductivity to increase. Further drying will lead to particle–particle contact and creation of a channel structure in the film. Further evaporation will close these channels, creating aqueous filled pockets within the film. Subsequently, the mobility of the ions, responsible for the electrical conductivity, will be reduced by collapse of these pockets. Conductance was measured using a 1286 electrochemical interface connected to a BBC computer. The electrodes were made using photolithography on resist coated double-sided copper clad board. A volume of 1 ml of latex was applied to the electrode using a draw down apparatus to produce a film of thickness 0.1 mm. The change in the conductivity was measured as the film dries. The applied voltage was 0.01 V and the initial resistance was 100 Ω. The time interval between analyses 30 s. The value of the voltage was selected to minimise heating of the latex, yet give the maximum sensitivity in the measurements.

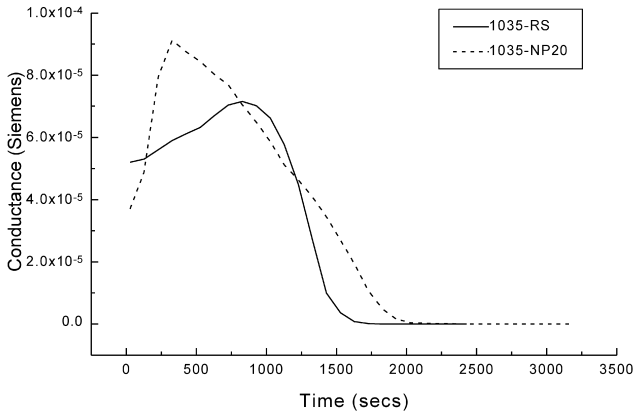

[A]

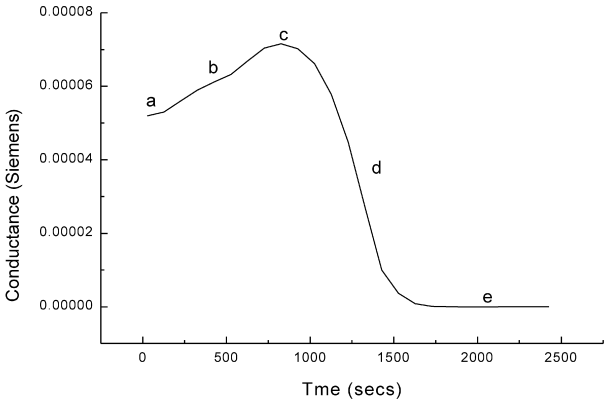

[B]

Fig. 1. (A) Conductance–time profile for 1035-RS and 1035-NP20; (B) model of conductance drying profile in 1035-RS and 1035-NP20 latexes.

2.2.2. Stages two and three of film formation—the maturation of latex films

When the latex film is macroscopically dry, other techniques can be applied to the characterisation of the films.

Dielectric spectroscopy. Analysis of the dielectric properties was carried out over the range 10^{-3}–6×10^{5} Hz and a temperature range from 270 to 355 K [2]. A coating of a silver loaded epoxy was used as the electrodes for the study.

3. Results and discussion

The analysis is divided into consideration of the drying process and the physical properties of the 'dry' latex once it has formed.

3.1. Drying process

3.1.1. Conductimetric analysis

Ionic conductance was measured during the drying process, Fig. 1(A) and a model of the profile, Fig. 1(B) were used to explain the observed behaviour. The latex in region (a) exists as stabilised dispersion of polymer particles dispersed in a dilute ionic solution. The ions are associated with residue form the initiators used in the latex preparation. Evaporation of water increases the ionic strength of the liquid between the particles and the conductivity consequently increased in region (b). A maximum in the conductance plot corresponds to a coincidence of the maximum ionic strength with a maximum mobility in region (c). The conductance starts to fall as the close packing of the particles increases the density of the stabiliser in between the particles and this impedes the movement of the ions in region (d). The conductance reaches a constant value indicating that ion movement is fully retarded on a macroscopic level and reflects a high level of stabiliser/particle interaction in region (e).

3.1.2. Dielectric spectroscopy under ambient conditions

Dielectric spectra were obtained for the two latexes over an extended aging period. Films were analysed at room temperature (~295 K) at various stages of aging, using dielectric spectroscopy over a frequency range of 10^{-1}–6×10^{4} Hz. The dielectric analysis was possible once the latex has formed a coherent film, this typically occurred ~24 h after casting of the liquid latex film. The dielectric permittivity and loss data for 1035-RS and 1035-NP20 are shown in Figs. 2 and 3. The dielectric data for 1035-RS reveal that there are several stages in the film maturation process. Initially, the permittivity and loss values are incredibly high indicating the presence of a combination of Maxwell Wagner Sillers [19,20] [MWS] and blocking electrode effects. Similar effects were observed in the study of 2-ethylhexylacrylate/methyl methacrylate copolymers latex materials [2]. The MWS contribution is attributed to water held in pockets and interstitial sites between particles, when no conductive path exists to the electrodes. The blocking electrode effects arise from the formation of layers of closely packed latex particles at the electrode surface inhibiting ion movement and discharge at the electrodes and is also associated with the work function for the electrode used. Both these processes have similar relaxation behaviour and are difficult to separate. For simplicity, in this paper both processes will be referred to as ionic dipole processes, reflecting the fact that the charge distribution generated in both cases creates very large effective dipole relaxation processes.

The permittivity for both latexes falls slowly over the first 24 h and then more markedly over the next 52 days. In the case of 1035-RS, a significantly reduced was observed in the ionic dipole process contribution after 52 days, Fig. 2(A)–(B). The fall in the ionic dipole process and conductivity contributions arise from loss of residual water, a restriction of the ion mobility and a change in the route which the ions followed to reach the electrode surface. The profile for the 1035-NP20 latex, Fig. 3(A)–(F) is very different from that for the 1035-RS latex. Although the

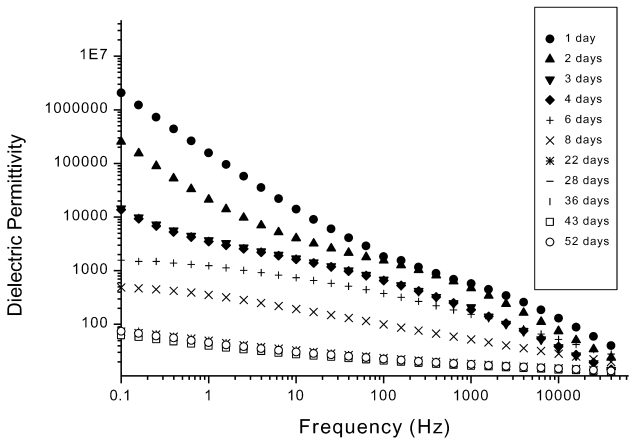

[A]

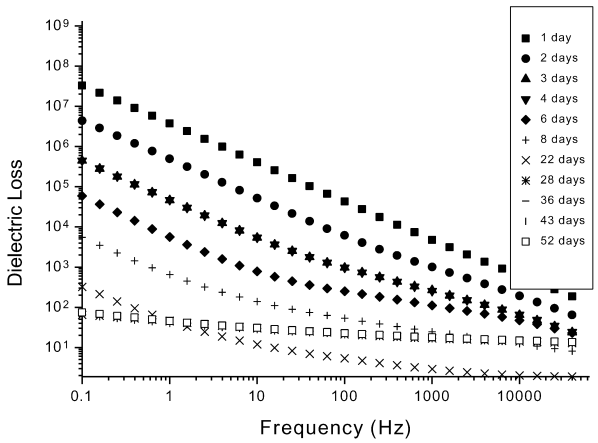

[B]

Fig. 2. Change in dielectric permittivity (A) and dielectric loss (B) with time for 1035-RS.

initial permittivity is high, indicating both MWS and blocking electrode contributions, their magnitudes fall markedly during the first 24 h of maturation. An ionic dipole relaxation process is seen at ca. 1000 Hz, which diminishes in intensity with age but remains at the same frequency. This type of behaviour is typical of a MWS process in which the latex structure responsible for the process is not changing but the number of such features is decreasing with time. Such a feature might be associated with conduction processes within closed channels. Evaporation of water and compaction of the latex will lower the ionic conductivity and shift the ionic dipole relaxation process to lower frequencies. Compaction of the latex particles will reduce the content and size of the inter-particle channels leading to a reduction in the amplitude of the ionic dipole process and a shift of the process to higher frequencies. Since both these processes occur concurrently, the relaxation process appears to be static on the frequency axis with time.

Over a longer period of aging, the permittivity is observed to fall, indicating that there is further loss of water and occluded structure as the film becomes more homogeneous. A dipole relaxation process associated with motion of the PEG chain was resolved which initially moves to lower frequencies with time, indicating a decrease in chain mobility, Fig. 3(A)–(F). However, the further loss of water causes the relaxation process to once more to move higher frequency, before again falling in frequency. This behaviour can be explained by assuming that the initial drop in the relaxation frequency is associated with the close approach of the latex particles increases crowding and slowing the motion of the chains. Further loss of water will cause the hydration sheath to be lost and this apparently increases the flexibility of the polymer chains. However, the closer packing of the latex particles will once more crowd the chains and slow the relaxation frequency down. Keintz et al. [18] studied surfactant desorption from latex particles using FTIR and postulated that the ethylene oxide chains of NP20 plasticise the outer particle membranes. It has also proposed that surfactant leaves the particle surface during film formation to penetrate the polymeric phase, the surfactant now having solubility similar to the matrix in which it is becoming dispersed. The bulk of the surfactant would attempt to desorb to the film–air and film–substrate interfaces and only a small amount, equal to the solubility limit, would take part in plasticisation. One of the most significant features in the dielectric data presented above is the change in permittivity as the samples age, Fig. 4. The differences between the permittivity time profiles of the two samples are marked and provide information on both the extent of retained water in the sample and its heterogeneity.

The permittivity of 1035-RS is much higher than that of 1035-NP20 and falls much more slowly over the aging period. A decrease in permittivity in these samples would indicate that residual water is being expelled and the boundaries between particles disappearing i.e. coalescence. Therefore, from Fig. 4 it can be concluded that coalescence in 1035-RS is inhibited. The permittivity–sample age profile of 1035-NP20 shows a much faster decrease than that for 1035-RS.

As two 1035-NP20 particles come into close contact their absorbed layers interpenetrate and the ethoxy chains of synperonic NP20 penetrate the outer particle membrane of a neighbouring particle promoting interparticle diffusion and the subsequent development of mechanical properties in the film, Fig. 5. As two 1035-RS particles come into close contact, these chains interpenetrate but are unable to achieve the same degree of coalescence as possible with synperonic. The formation of crystallites in the PEG phase and the restriction of the motion of the surfactant chains to a single polymer particle cause the observed retarded penetration. Synperonic NP20 has an ethoxy chain 20 units long and an effective melt temperature of 305 K. However, 1035-RS has an equivalent molar mass of 1760 in the hydrophilic chain and a melting point of 322 K and hence a greater tendency to form crystalline phases between the particles.

The dielectric data was analysed using the Havriliak and

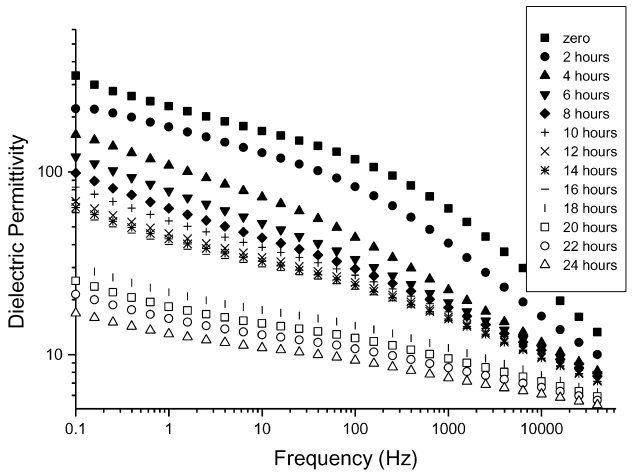

[A]

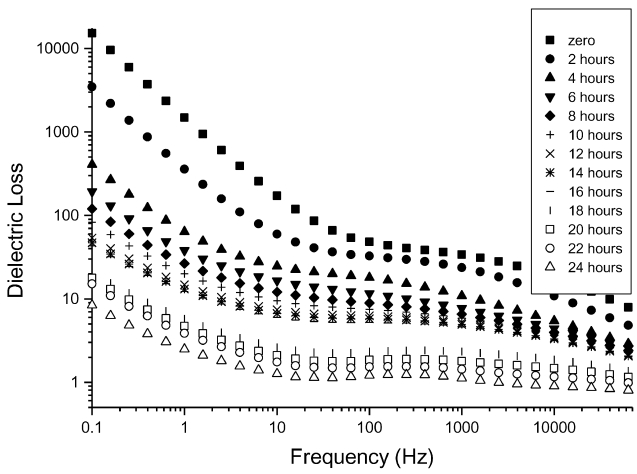

[B]

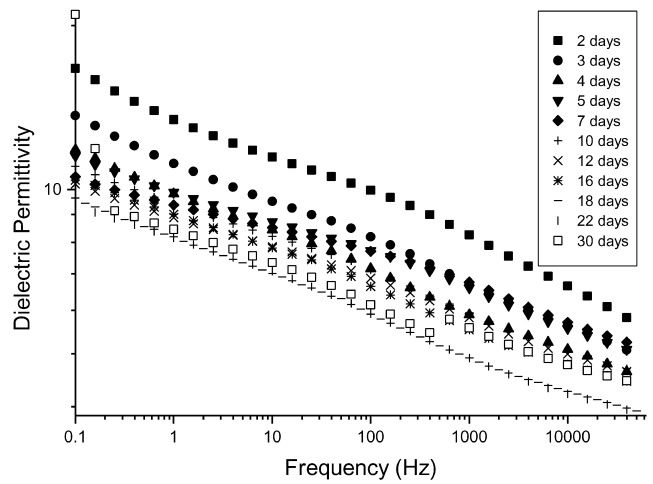

[C]

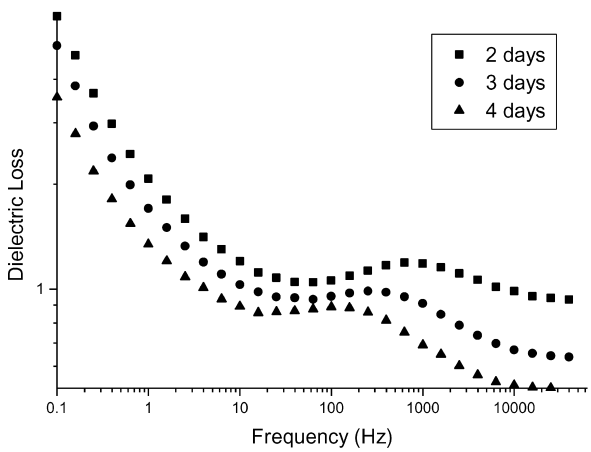

[D]

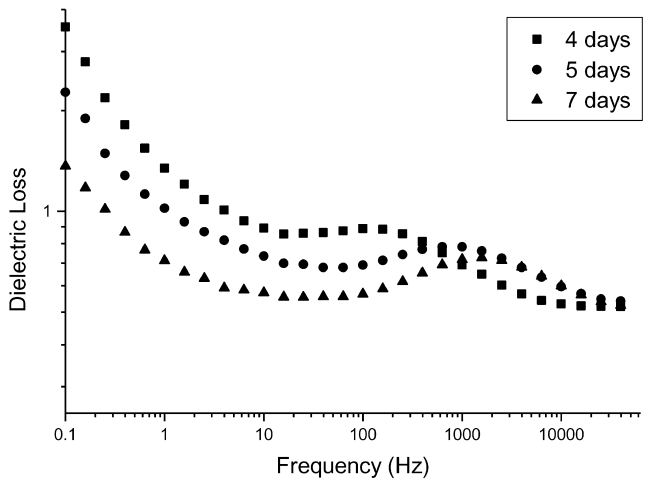

[E]

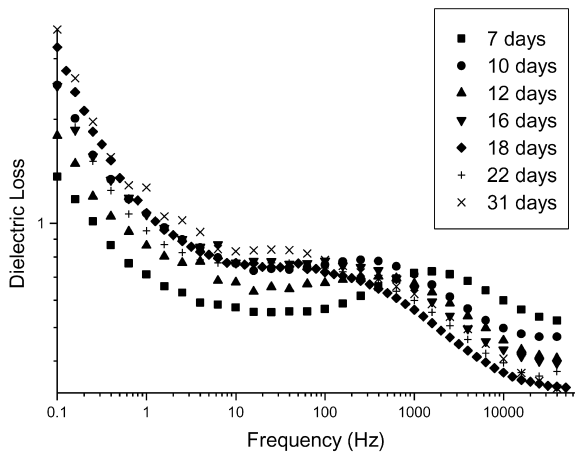

[F]

Fig. 3. Change in dielectric permittivity (A) and dielectric loss (B) with time for 1035-NP20 for the first time interval; the change in dielectric permittivity (C) and dielectric loss (D–F) with time in the second time interval.

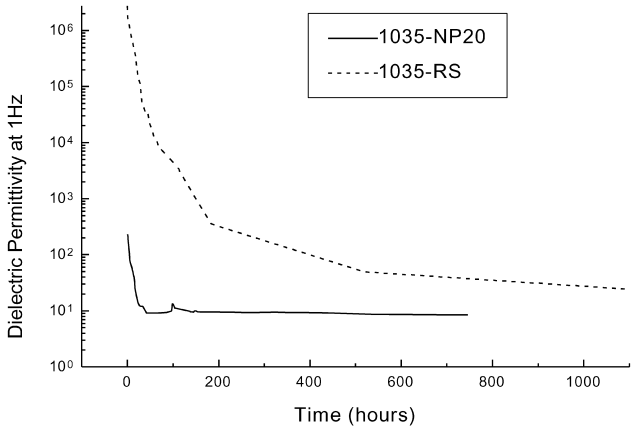

Fig. 4. Change in dielectric permittivity (1 Hz) with sample age.

Negami analysis [21]

$$\varepsilon^*(\omega) = \varepsilon_\infty + \frac{(\varepsilon_s + \varepsilon_\infty)}{(1 + (i\omega\tau)^{1-\alpha})^{1-\beta}} \quad (1)$$

where α and β are temperature dependent, dimensionless constants and are independent of frequency. The β value was found to be ~ 1 for all stages of maturation and a plot of the change in α as the sample age are shown in Fig. 6.

The conductivity and ionic dipole process contributions in 1035-RS initially mask any relaxation processes and α and β values could not be determined for the first 5 days of maturation. The aging period of 6–52 days shows a steady decrease in the value of α indicating that the distribution of processes occurring in the system are increasing as the sample ages. Inspection of the dielectric permittivity and loss data for the aging period 6–52 days indicates that in this region the conductivity and ionic dipole process contributions are declining, however, the loss values remain very high suggesting that these processes are still present and dominant. The decline in α may be attributed to the unmasking of dipolar processes, as the conductivity and ionic dipole process are reduced. As these contributions gradually diminish, the presence of side chain rotation and T_g related relaxation processes become evident.

The plot of α with respect to age for 1035-NP20 shows a complicated profile. The value for α is initially high, but falls sharply over the first 2 days of aging. Over the period 2–7 days, α rises sharply and then subsequently falls again.

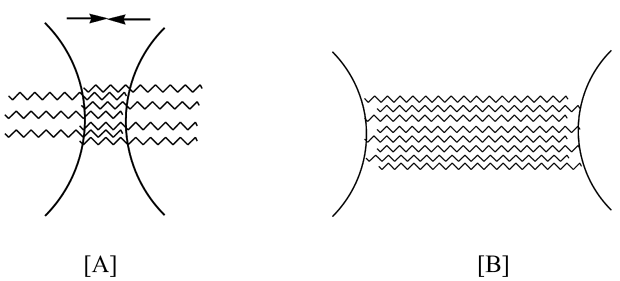

Fig. 5. Schematic of close particle contact in (A) 1035-NP20 and (B) 1035-RS.

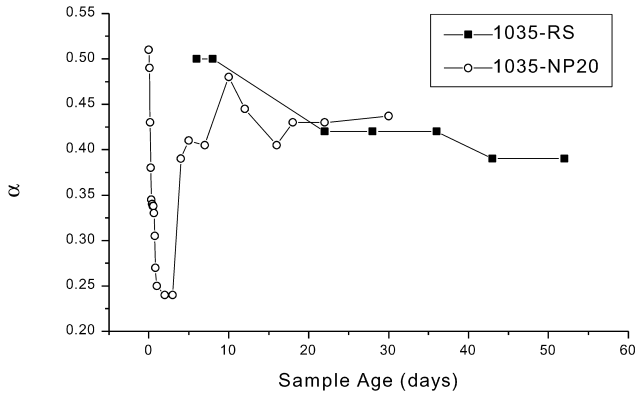

Fig. 6. Plot of α values against sample age for 1035-RS and 1035-NP20.

The initial sharp decline in α can again be attributed to the decline in conductivity and ionic dipole process contributions resulting in the unmasking of the dipole relaxation. Disorder of the ethoxylate chains in the aqueous phase will be consistent with the concept of entropic stabilisation. As coalescence is approached so closer chain packing must occur and hence a more uniform distribution of chain elements will be generated reflected in a higher value of α.

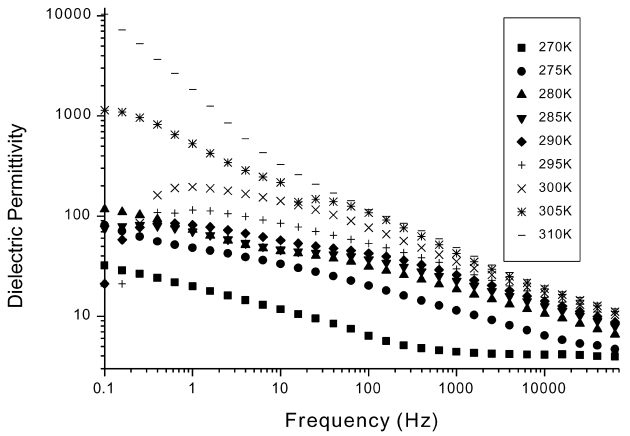

[A]

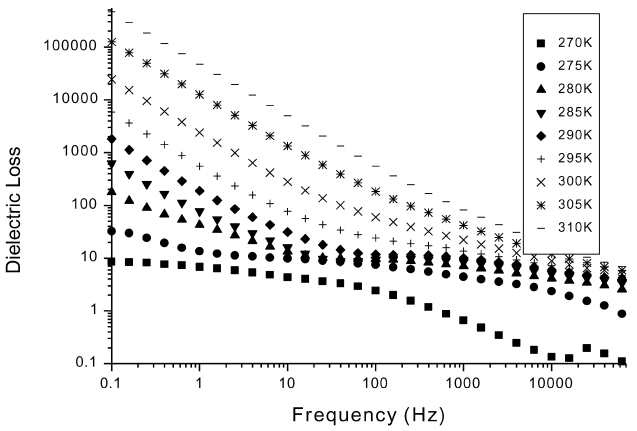

[B]

Fig. 7. Dielectric permittivity and loss for 1035-RS sample at zero time.

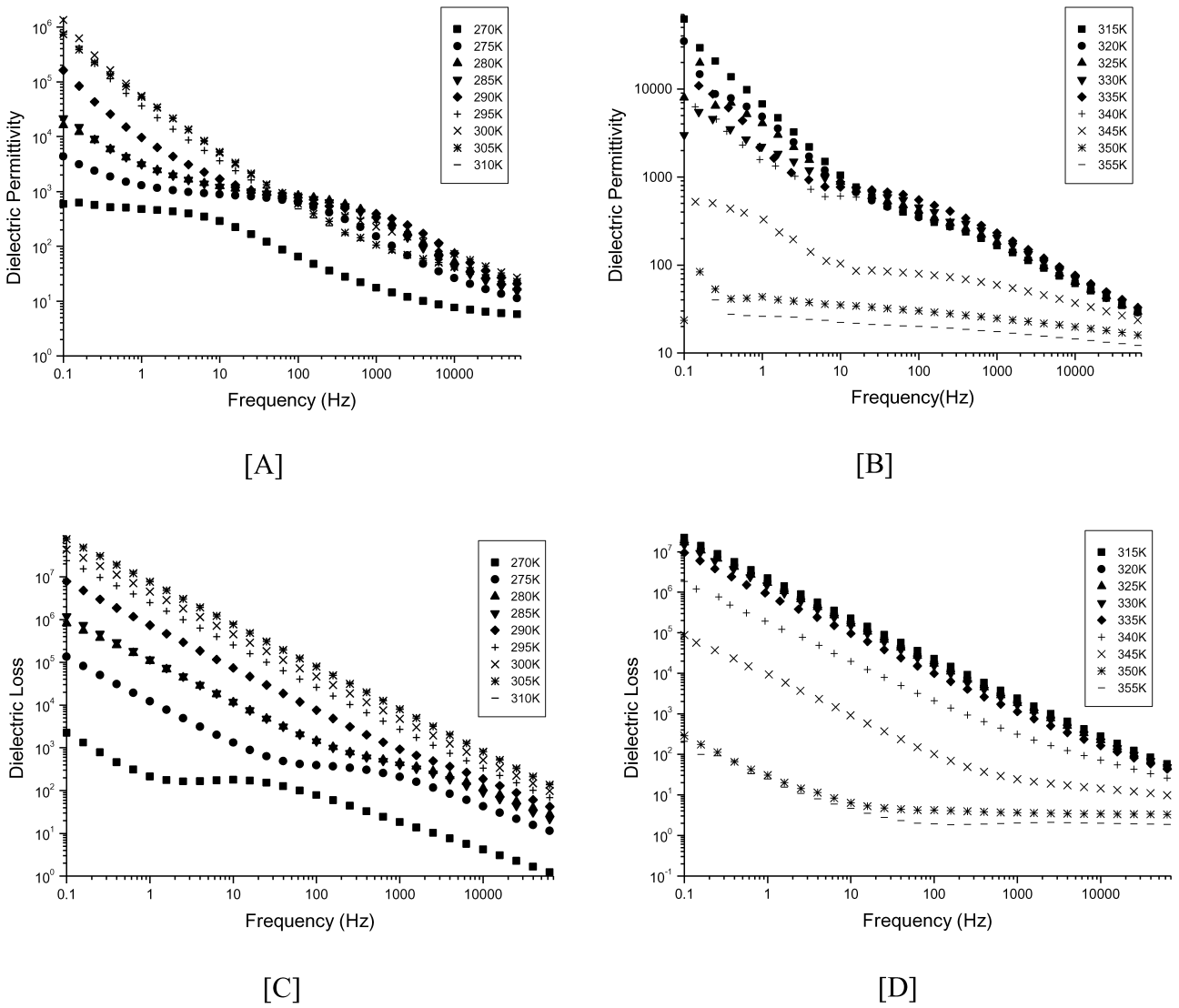

Fig. 8. Dielectric permittivity and loss in 1035-NP20 aged for zero time.

A subsequent decrease in α is consistent with the idea of the PEG chains penetrating the polymer latex particle. Considering the dielectric loss data shown in Fig. 3(F), a relaxation is observed to move to lower frequencies and then to shift to higher frequencies.

3.1.3. Dielectric thermal analysis

Dielectric thermal analysis was carried out in an attempt to shed light on the nature of the dipole relaxation process. Films of the two latexes were cast and analysed at various stages of aging. Data was collected over a frequency range of 10^{-1}–6×10^4 Hz and a temperature range of 270–355 K at an interval of 5 K. The temperature was equilibrated for 30 min before measurements were taken. An example of the type of data obtained is shown in Figs. 7 and 8 for unaged samples.

The 1035-RS data was characterised by the retention of a strong conductivity and ionic dipole process contribution at all stages of maturation and indicates that close packing and coalescence was inhibited. Although 1035-NP20 shows a higher initial conductivity and ionic dipole process contribution; this falls off much more rapidly than seen in 1035-RS, which supports the ambient condition measurements.

A plot of the permittivity at 1 Hz for each sample at the stages of aging monitored allows the coalescence temperature to be determined from the maximum permittivity at 1 Hz over the temperature range scanned, Fig. 9. The decline in permittivity is associated with a morphology change and the peak is assigned to the coalescence temperature. Water loss, plasticisation and surfactant–polymer interactions, can influence the coalescence temperature. Data were obtained at 6 day intervals over a period of 36 days and were very similar to those shown in Figs. 7 and 8 except that due to aging the amplitudes of the processes were changed as the ionic processes were lost due to drying of the film. The coalescence temperature of 1035-NP20 rises over the first few days of aging, probably a result

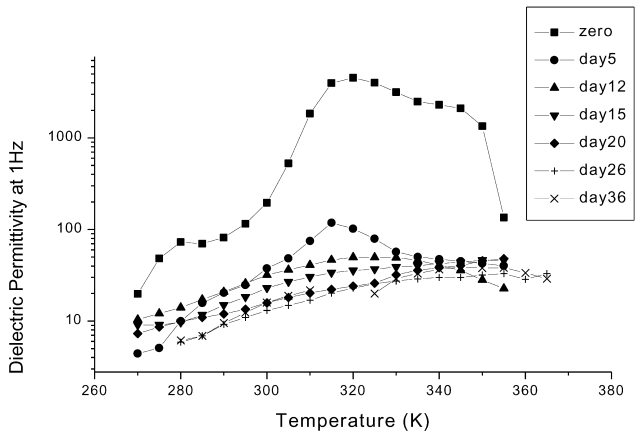

[A]

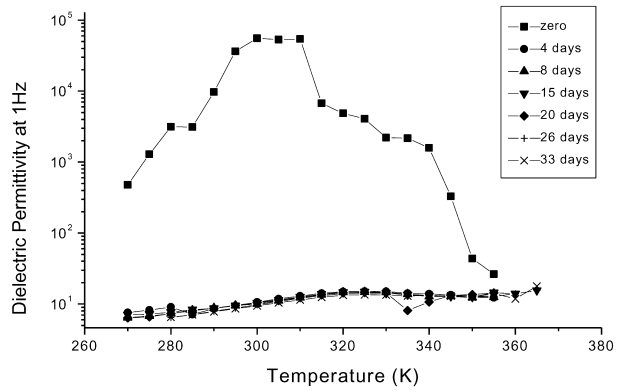

[B]

Fig. 9. Permittivity–temperature plots for 1035-RS and 1035-NP20.

of water (an internal plasticiser) loss from the system. The coalescence temperature then remains constant over the period of aging measured, 36 days. In contrast, the coalescence temperature of 1035-RS is low initially and then rises sharply after 12 days of aging.

Initially, the coalescence temperature of 1035-RS is lower than that of 1035-NP20, which is consistent with the assumption that there is a larger amount of water retained in the sample. Water acts as an internal plasticiser and consequently its loss leads to an increase in the T_g of the polymer film. Dielectric measurements performed under ambient conditions show that 1035-NP20 expels residual water much faster than 1035-RS and attains a higher initial coalescence temperature.

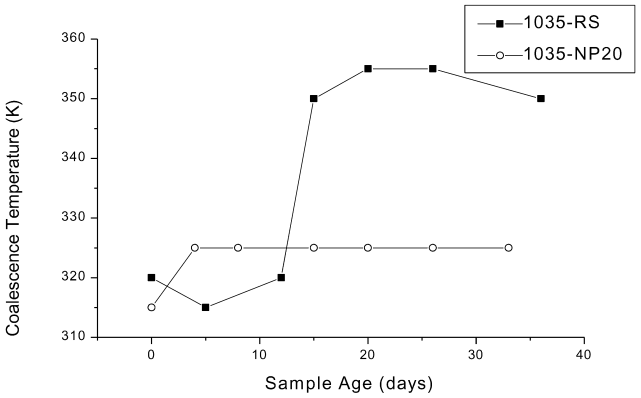

Fig. 10. Plot of variation in coalescence temperature with sample age.

Both samples show a constant coalescence temperature over the final stages of aging. However, 1035-RS exhibits a coalescence temperature that is 35 K higher than 1035-NP20, which is surprising considering the close similarity in the compositions of these materials. The difference in coalescence temperatures for the two latexes can be attributed to surfactant effects. Heating the sample promotes coalescence and the amount of energy required reflects the particles resistance to deformation and the extent to which crystalline domains are formed in the interparticulate region.

Examination of the permittivity–temperature curves for 1035-NP20, showed a decrease in permittivity at 325 K, indicating a change in morphology. There are subsequent changes at higher temperatures indicating that although coalescence may have occurred through out the bulk of the film, some interfaces between particles have been retained which are only lost on subsequent heating. The variation of the coalescence temperature with ageing time is presented in Fig. 10.

The dielectric data for the two latexes indicates how the intrinsic mobility reflected in the dipole relaxation changes on ageing. The activation energies change with ageing time and for 1035-RS; the value initially was observed to be 104 ± 10 kJ mol^{-1}, after 5 days the activation energy has dropped to 67 ± 1 kJ mol^{-1}. Subsequently, after 12 days a value of 140 ± 16 kJ mol^{-1} was observed, after 15 days the value was 187 ± 15 kJ mol^{-1}, after 20 days the value was 50 ± 1 kJ mol^{-1} and after 26 days it had become 133 ± 17 kJ mol^{-1} and was finally 200 ± 12 kJ mol^{-1} after 36 days. These changes in value reflect the way in which the environment varies with time. The values of the activation energy are relatively low and of the order expected for side chain motions. Similar values were obtained for 1035-NP20. The initial activation energy being 116 ± 15 kJ mol^{-1}, after 4 days it has increased to 229 ± 58 kJ mol^{-1} and dropped to 108 ± 8 kJ mol^{-1} after 8 days. After 15 days the value had increased to 214 ± 12 kJ mol^{-1} and then drops to 90 ± 10 kJ mol^{-1} after 20 days and finally increases to a value of 142 ± 8 kJ mol^{-1} after 36 days.

4. Conclusions

Comparison of the behaviour observed in the drying of Synperonic NP20 and the reactive surfactant reveal interesting features that reflect the influence of stabiliser structure on the coalescence process. Mechanical

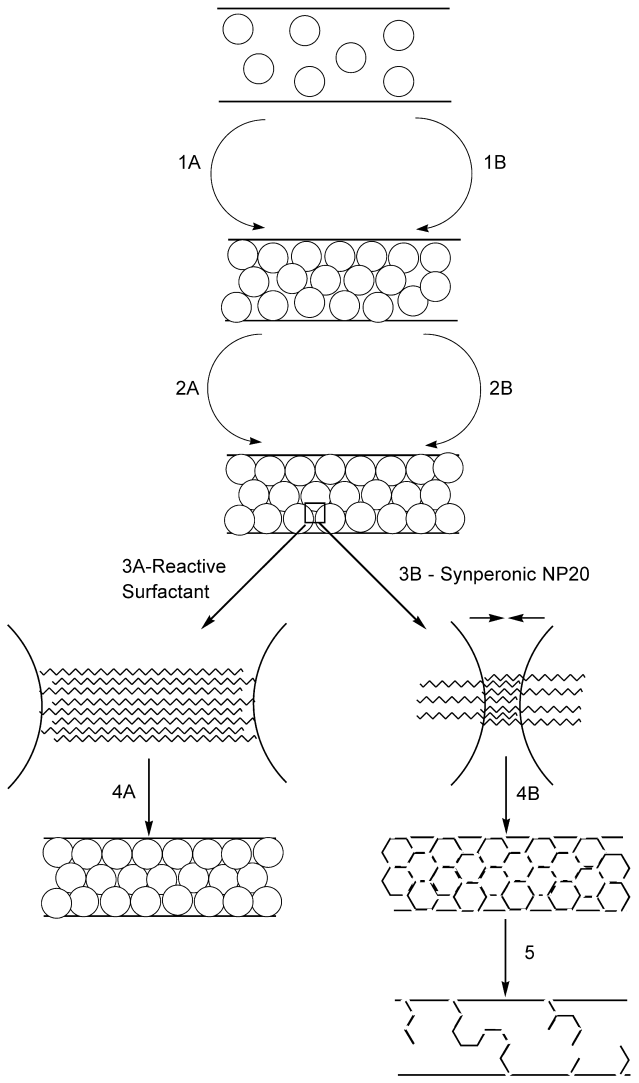

Fig. 11. Model of film formation in latexes stabilised by Synperonic NP20 and the reactive surfactant.

measurements of drying show that both latexes exhibit a single stage drying profile indicative that at ambient temperature they are above their MFFT. The drying rates were essentially those of water evaporation.

Dielectric spectroscopy measurements performed under ambient conditions show that coalescence in 1035-RS is inhibited, this is revealed by the retention of the MWS and conductivity contributions over extended aging periods. The coalescence in 1035-NP20 is promoted, indicated by the rapid decline in the ionic dipole process and conductivity contributions in the early stages of aging. The subsequent emergence of a series of dipolar relaxations gave further indications of coalescence as these were assumed to be associated with water loss, plasticisation and the establishment of the films mechanical properties. These differences in behaviour can again be attributed to the surfactant layer. Synperonic NP20 is known to plasticise the latex particles membrane and it is therefore reasonable to assume that its presence in the latex film would assist coalescence. Inhibition of coalescence by the reactive surfactant was deemed to occur by formation of regions of crystalline PEG formed by an increase in the local concentration of ethoxylate chains between the latex particles.

This analysis was supported by dielectric thermal analysis, which allowed a coalescence temperature for the two latexes over the aging period to be determined. The results show that although the latexes have comparable T_gs and MFFTs, 1035-RS has a coalescence temperature ~30 K higher than 1035-NP20 indicating that coalescence is inhibited in this sample, Fig. 10.

The film forming process can be modelled [22], Fig. 11. In the model, the route denoted by the letter A signify the latex stabilised by the reactive surfactant, the route denoted by B signify the latex stabilised by synperonic NP20. Evaporation of water to form a dense array of spheres is depicted in stage 1A. The lack of mobility of the reactive surfactant and its long ethoxy chain length lead to the formation of crystalline region between particles at this stage. The formation of these regions assists the establishment of mechanical properties and also presents a smaller surface area for hydration. These factors result in a faster rate of film formation. Evaporation leads to a dense array of spheres depicted ion stage 1B, however, the surfactant chains have greater mobility and do not form regions of crystallinity. The ethoxylate chains of synperonic NP20 have more freedom and can become hydrated, this occurs to a greater extent than in crystalline regions due to the increased surface area which is available. More energy is required to remove bound water from the ethoxylate chains and therefore the drying rate is slower. Once a film has formed the latex tries to expel residual water and deform to fill available space, depicted in stage 2A. However, the presence of crystalline regions between particles prevents the latex particles from close packing and inhibits deformation. The crystalline region presents a physical barrier to close packing and deformation and as a consequence therefore expulsion of residual water is very slow.

The ethoxylate chains of synperonic NP20 are very mobile and present no barrier to close packing, depicted in stage 2B. Therefore, as the ethoxylate chains slide past each other, the latex particles can close pack and expel residual water rapidly. As the films age, sometimes referred to as ‘further coalescence’ or ‘maturation’ the arrangement of ethoxylate chain between particles becomes more ordered and the degree of crystallinity increases, therefore, the barrier to coalescence becomes stronger, depicted in stage 3A. The synperonic NP20 chains can easily slide past each other at room temperature, allowing close packing. Additionally, the ethoxylate chains are soluble to a certain extent in the particle membrane and can plasticise the molecules in the interface and aid deformation of the particles, depicted in stage 3B. The presence of crystalline domains between latex particles, caused by the reactive surfactant inhibits close packing to such an extent that

deformation of the latex particles cannot occur, depicted in stage 4A. Hence, subsequent interpenetration of the polymer chains is prevented and the particle identities remain intact. Additionally, because the surfactant molecules are tethered to the particle surface, the formation of a rigid crystalline region will also inhibit the motion of the latex polymer chains. The resultant effect will be an increase in the T_g of the outer particle membrane that will further impede coalescence. Plasticisation of the latex particle membrane by synperonic NP20 will assist deformation, depicted in stage 4B. Additionally, plasticisation increases the mobility of the latex polymer chains and so interparticle diffusion will be promoted.

Deformation and subsequent interparticle diffusion leads to a relatively homogeneous film. Some particle boundaries may be retained, but these will disappear over time, depicted in stage 5.

The main conclusion which can be drawn from this study is that the presence of the reactive surfactant inhibits latex particle coalescence whereas synperonic NP20 promotes coalescence. This phenomena is the result of two factors; first, the restriction of the reactive surfactant to the particle surface and secondly, the effects of the length of the hydrophilic chain. It is reasonable to assume that both tethered or untethered, long polyether chains will be able to form crystalline domains that will inhibit coalescence.

Acknowledgements

One of us (LC) wishes to thank the EPSRC and ICI (Paints) for the support of a CASE studentship for the period of this research. We wish to thank Dr David Taylor and Dr David Elliott for their help and guidance during the course of this study.

References

[1] Cannon LA, Pethrick RA. Comparison of the effect of reactive and non-reactive steric stabilizers on the mechanism of film formation in methyl methacrylate/butyl aerylate copolymers latexes. Part 1. Differential scanning calorimetry, dynamic mechanical analysis and atomic force microscopy. Submitted for Publication.
[2] Cannon LA, Pethrick RA. Macromolecules 1999;32:7617.
[3] Eckersley ST, Rudin A. In: Provder T, Winnik MA, Urban MW, editors. Film formation in waterbourne coatings. ACS symposium series 648, vol. 2.; 1996.
[4] Niu BJ, Martin LR, Tebelius LK, Urban MW. In: Provder T, Winnik MA, Urban MW, editors. Film formation in waterbourne coatings. ACS symposium series 648, vol. 301. Washington, DC: American Chemical Society; 1996.
[5] Keddie JL, Meredith P, Jones RAL, Donald AM. In: Provder T, Winnik MA, Urban MW, editors. Film formation in waterbourne coatings. ACS symposium series 648, vol. 332. Washington, DC: American Chemical Society; 1996.
[6] Eu M-D, Ullman R. In: Provder T, Winnik MA, Urban MW, editors. Film formation in waterbourne coatings. ACS symposium series 648, vol. 79. Washington, DC: American Chemical Society; 1996.
[7] Winnik MA. In: Provder T, Winnik MA, Urban MW, editors. Film formation in waterbourne coatings. ACS symposium series 648, vol. 51. Washington, DC: American Chemical Society; 1996.
[8] Routgh AF, Russel WB. AICHE J 1998;44(9):2088.
[9] Feng JR, Winnik MA. Macromolecules 1997;30(15):4324.
[10] Wang YC, Winnik MA. J Phys Chem 1993;97(11):2507.
[11] Winnik MA, Winnik FM. Advances in chemistry series 236. Washington, DC: American Chemical Society; 1993. p. 485.
[12] Sperry PR, Snyder BS, O'Dowd ML, Lesko PM. Langmuir 1994;10:2619.
[13] Keddie JL, Meredith P, Jones RAL, Donald AM. Macromolecules 1995;28:2673–82.
[14] O'Callaghan KJ, Pain AJ, Rudin A. J Polym Sci, Part A: Polym Chem 1995;33(11):1849–57.
[15] Rodriguez F. Principles of polymer systems, 2nd ed. New York: Wiley; 1992.
[16] Mahr TG. J Phys Chem 1970;74:2160.
[17] Bevan MA, Price DC. Langmuir 2000;16:9274.
[18] Keintz E, Holl Y. Colloids Surf A—Physicochem Engng Asp 1993;78:255–70.
[19] Van Beek LKH. Prog Dielectr 1967;7:69.
[20] Sillers RW. Inst Electr Engrs 1937;80:378.
[21] Havriliak S, Havriliak SJ. Dielectric and mechanical relaxation in materials. New York: Hanser; 1997.
[22] Cannon L. PhD Thesis. University of Strathclyde; 1998.